

Because the Simplified Theory of Plastic Zones to be developed in this book is mainly useful for application to elastic-plastic structural behavior under variable loading, some phenomena of structural behavior relevant to the life of a structure are discussed in this chapter. Particular emphasis is placed on the phenomenon of ratcheting.

## 2.1 Local and Directional Stress Redistribution

The obvious important points of plastic material behavior at monotonic loading are greater distortions and lower stresses than with linear elastic behavior. Local and directional stress redistributions are often caused in structures by interacting in accordance with field equations, i.e., equilibrium and compatibility conditions (kinematic conditions).

“Local” stress redistribution means that the relationship between the stresses at different locations of the structure is changed as a result of plastic material behavior. Thus, structural parts that appear lowly stressed in an elastic calculation can in fact be highly stressed, or stresses may exhibit different signs at the same location in elastic or plastic calculations. This phenomenon is likely to be familiar to many students from lectures about plastic hinge theory and can, for example, easily be recognized in a *T*-shaped beam cross-section under bending (Fig. 2.1). Cross-section fibers just above the neutral axis are in compression with elastic material behavior, but under tension with plastic material behavior.

In multiaxial stress states it may happen that, in addition to their absolute values, the ratios of the stress components to each other change because of plastic behavior compared to linear elastic behavior. In deviatoric stress space, this manifests itself as a change in angle of the position vector of the stress state and is referred to as directional stress redistribution.

A simple example of this is shown in Fig. 2.2, where a differentially small material volume or finite element is subjected to a plane stress state (stress is zero in the *z*-direction). In one direction a displacement-controlled loading is applied,

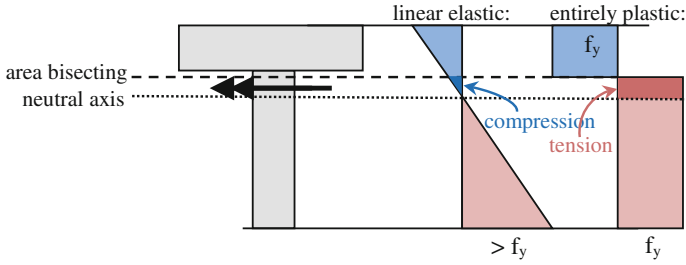


**Fig. 2.1** Local redistribution of axial stresses in a *T*-shaped beam cross-section under uniaxial bending (qualitative representation)

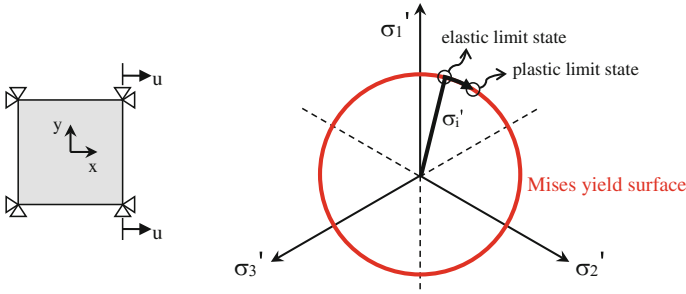


**Fig. 2.2** Directional stress redistribution in plane stress state and monotonically increasing displacement-controlled loading in case of non-hardening material

whereas in the other direction any shift of the bearing is prevented, so that a plane strain condition exists (strain is zero in the  $y$ -direction). Because of the homogeneous stress condition, this is strictly speaking a material problem, not a structural problem.

The stress state is given by

$$\sigma_i = \begin{pmatrix} \sigma_1 \\ \nu \sigma_1 \\ 0 \end{pmatrix} \rightarrow \sigma'_i = \frac{1}{3} \begin{pmatrix} 2 - \nu \\ -1 + 2\nu \\ -1 - \nu \end{pmatrix} \sigma_1. \quad (2.1)$$

The Poisson's ratio in steel is approximately  $\nu = 0.3$  for elastic behavior. The incompressibility assumption for the plastic portion of the total strain given by Eq. (1.16) corresponds to  $\nu^{\text{pl}} = 0.5$ . After exceeding the yield stress, the effective Poisson's ratio for elastic-plastic behavior increases gradually from 0.3 to 0.5 in the plastic limit state for a non-hardening material at infinitely high load level. Thus, the ratio of the stress components varies from  $1 : 0.3 : 0$  to  $1 : 0.5 : 0$ , and the ratio of the deviatoric stress components from  $1 : -0.235 : -0.765$  to  $1 : 0 : -1$ .

It is left to the reader to imagine the impact of hardening for this example of monotonous loading which, because of the directional stress redistribution, is different with kinematic and isotropic hardening.

In the present case, the directional stress redistribution occurs because of the difference in Poisson's ratio of elastic and plastic behavior. However, directional stress redistribution may also occur for a Poisson's ratio of 0.5 (elastic incompressibility). For this purpose, however, an inhomogeneous multiaxial stress state is necessary.

## 2.2 Structural Ratcheting Based on a Two-Bar Model

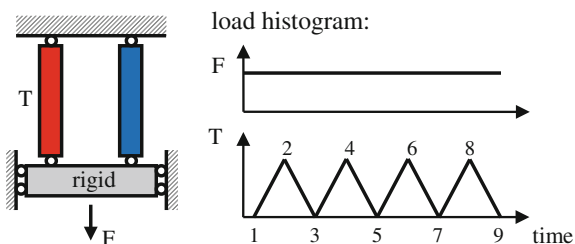
If the load is variable rather than increasing monotonically, ratcheting or progressive deformation may occur as already mentioned in Sect. 1.2.8. This phenomenon can be illustrated with reference to a two-bar model (Fig. 2.3) serving as a standard example of structural ratcheting, investigated analytically and experimentally by numerous authors, including dimension variations (different lengths and different cross-sectional areas of the two bars), multiple load variants (pulsating or alternating thermal loading), without and with kinematic and isotropic hardening, for example by Miller [1], Mulcahy [2], Jiang and Leckie [3], and Ponter [4]. The two-bar model is sometimes also referred to as the three-bar model, where the bars are arranged symmetrically, have symmetrical properties, and are loaded symmetrically. The results are then the same as described in the following.

Two parallel bars of the same length, same cross-section, and same material are connected by a rigid plate so that both bars are always equal in length (Fig. 2.3).

Linear elastic-perfectly plastic material behavior with temperature-independent material parameters is considered first. Small strains and small displacements are assumed, so that a change in the cross-sectional area caused by the load does not need to be considered and the equilibrium condition may be formulated at the undeformed system. First of all, a force  $F$  is applied, acting constantly in the following and causing a so-called primary stress  $\sigma_p$  of equal magnitude in both bars. In order not to exceed the plastic limit load, this stress must be less than the yield stress. In the left bar, a cyclic temperature change  $T$  is then applied whereas the temperature in the right bar remains constant.

In the heating phase, the free thermal expansion strain  $\varepsilon^{\text{th}}$  of the left bar is hindered so that compressive stresses occur whereas the right bar experiences tensile stresses of equal amount for equilibrium reasons. The arithmetic mean of the

**Fig. 2.3** Two-bar model subjected to cyclic loading



stresses in the two bars is the primary stress at any time,<sup>1</sup> so the stresses in the two bars can deviate from this by the same amount with different signs:

$$\Delta\sigma_{\text{left}} + \Delta\sigma_{\text{right}} = 0. \quad (2.2)$$

Because of the lack of hardening, not only is the maximum stress in each of the two bars fixed,

$$\sigma_{\text{max}} = f_y, \quad (2.3)$$

but also the minimum possible stress

$$\sigma_{\text{min}} = 2\sigma_P - f_y. \quad (2.4)$$

Because the rods are always equal in length, the following must apply at all times:

$$(\varepsilon^{\text{th}} + \varepsilon^{\text{el}} + \varepsilon^{\text{pl}})_{\text{left}} = (\varepsilon^{\text{el}} + \varepsilon^{\text{pl}})_{\text{right}}. \quad (2.5)$$

So we can identify stresses and strains in both bars at each point in the load histogram (Fig. 2.4).

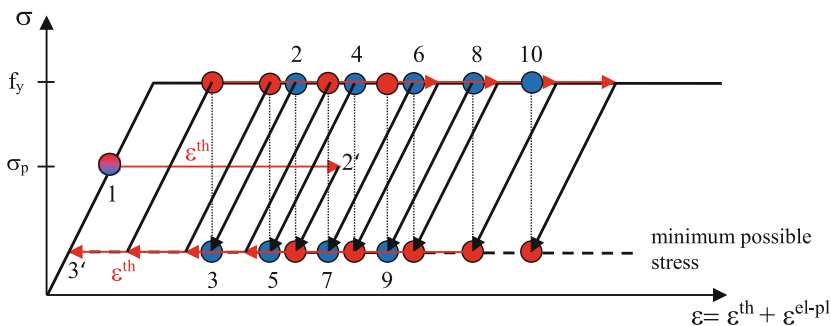
Starting from point 1, where both bars have the same stress  $\sigma_P$  below the yield stress  $f_y$ , the free thermal expansion  $\varepsilon^{\text{th}}$  is applied in the left bar (point 2' in the stress–strain diagram of Fig. 2.4). To maintain equal length in both bars, the mechanical strain must decrease in the left bar and increase in the right. According to the material law, the relief of the left bar can be only purely elastic, causing a reduced stress there, whereas the stress of the right bar increases because of equilibrium, but at most until the yield strength  $f_y$  is reached. Because the stress cannot rise any further, the stress in the right bar is known. At time 2, both bars are at the same thermo-elastic strain. The left bar still remains elastic, whereas the right bar is already plasticized.

In the next half cycle, the free thermal expansion  $\varepsilon^{\text{th}}$  in the left bar is withdrawn (point 3' in the stress–strain diagram). To enforce equal length in both bars, the left bar must become longer, the right bar shorter. The unloading in the right bar occurs purely elastically, whereas the stress in the left bar increases, associated with elastic action, until the stress reaches the yield stress, and then remains constant, whereas its expansion continues to increase. Because at time 3 no free thermal expansion is present, both bars have the same mechanical strain, and there is equilibrium. In this half cycle the left bar is plasticized whereas the right has undergone an elastic relief.

---

<sup>1</sup>The term “time” is not used here in the sense of a physical quantity, but only as an ordering quantity for successive operations. In the literature it is sometimes referred to as “pseudo-time”. The term “histogram” is to be understood in the same sense.

stress–strain diagram:



strain histogram:

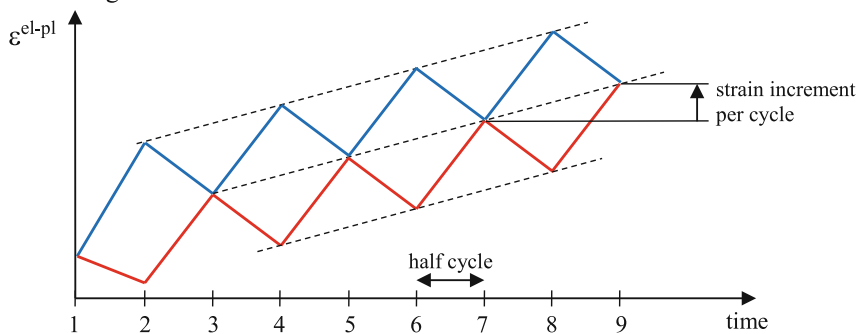


**Fig. 2.4** Structural ratcheting with the two-bar model as a result of cyclic loading in case of non-hardening material

In the same way, the development of stresses can be constructed for all further half cycles. After the first load cycle, the strain in the two bars increases with a constant strain increment in every cycle. If the theory of large displacements and large strains were applied, the cross-sectional area would decrease with the number of cycles because of the lateral contraction produced by the axial extension, and the strain would overproportionately increase with the number of cycles.

As a result of the cyclic loading, plastic axial hinges are alternately active in both bars in two successive half cycles, leading to a net increase of plastic strains (a strain accumulation according to Eqs. (1.32) and (1.33)) in each loading cycle.

## 2.3 Influence of Kinematic Hardening

Taking account of hardening in place of the linear elastic-perfectly plastic material model considered in the previous section, the strain increment per cycle changes in each load cycle. In the case of an unlimited kinematic hardening material, this strain increment decreases monotonically until it completely ceases after a finite or an infinite number of cycles, so that the structural response is eventually periodic.

Strain amplitudes occurring in each half cycle are then of the same absolute values but of opposite sign in two consecutive half cycles. It is said that the system has reached the state of shakedown. If only purely elastic changes of strain take place, we speak of elastic shakedown and of plastic shakedown in the case of elastic-plastic strain amplitudes.

For linear elastic-perfectly plastic material behavior, one needs only to distinguish between elastic shakedown, plastic shakedown, and ratcheting. If ratcheting occurs, theoretically infinitely large strains are achieved because of the constant strain increments after an infinite number of cycles. With hardening, however, we may initially get an accumulation of strain with each load cycle, so that a ratcheting mechanism exists, but coming to a halt after a number of cycles. It is then sometimes called finite ratcheting (Mulcahy [2]).

The two-bar model with linear kinematic hardening treated in the previous section has already been investigated in [1, 2]. For a hardening ratio  $E_p/E = 0.05$ , a primary stress  $\sigma_p/f_y = 0.8$ , and two different levels of cyclically applied temperature in the left bar, the histograms of the total elastic-plastic strain and the plastic portion of the strain, respectively, are shown in Figs. 2.5 and 2.6. A pulsating elastically

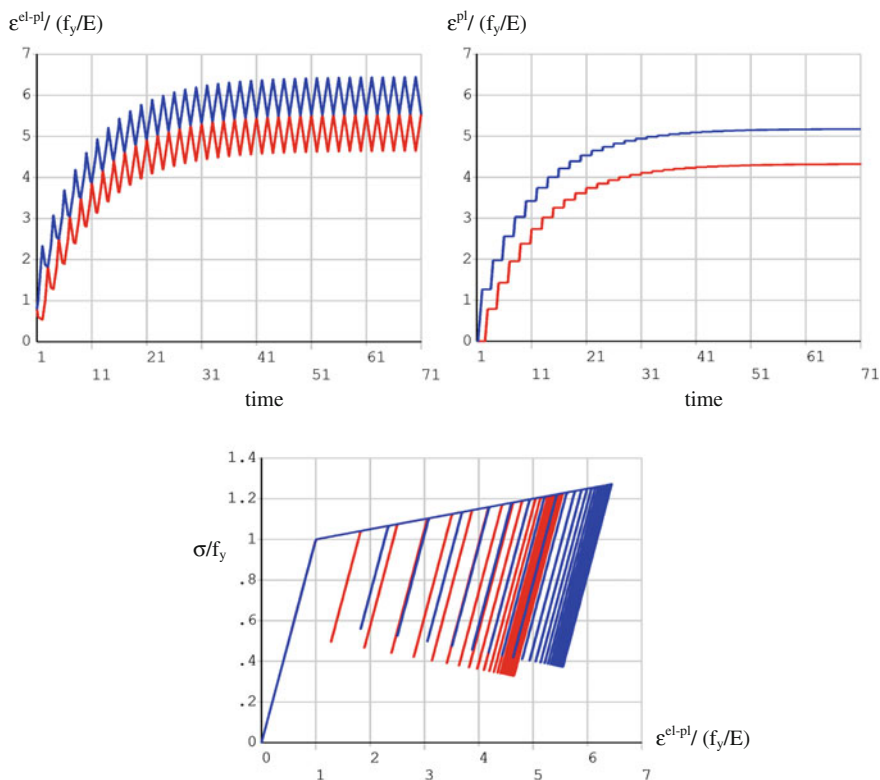


**Fig. 2.5** Progressive deformation in the two-bar model with linear kinematic hardening; elastic shakedown ( $\sigma_p/f_y = 0.8$ ;  $\sigma_r/f_y = 0.9$ ;  $E_p/E = 0.05$ )

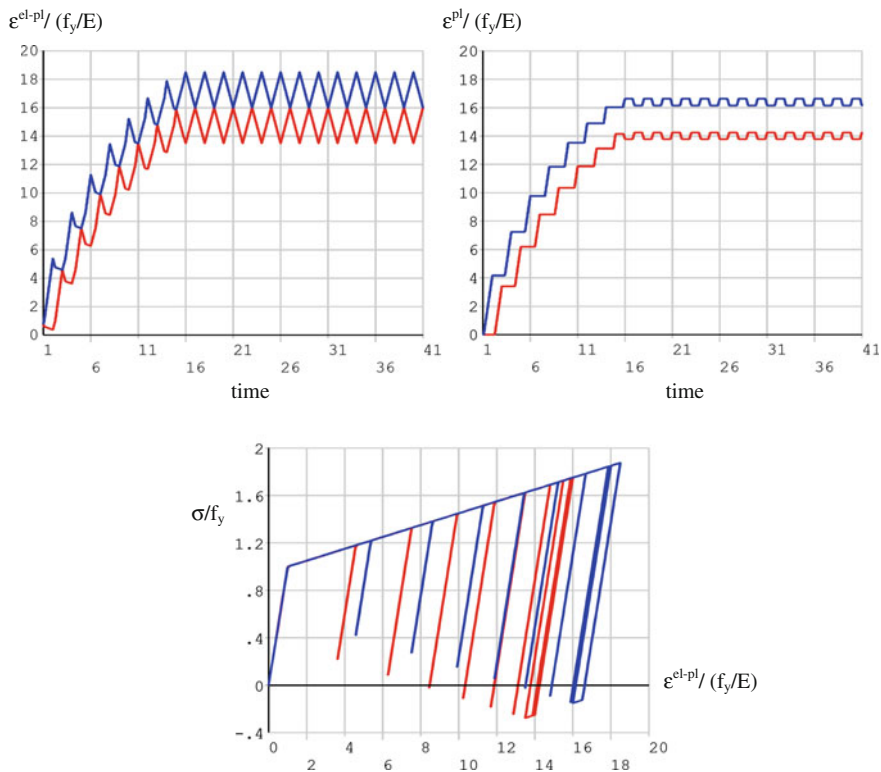


**Fig. 2.6** Progressive deformation in the two-bar model with linear kinematic hardening; plastic shakedown ( $\sigma_P/f_y = 0.8$ ;  $\sigma_T/f_y = 2.5$ ;  $E_r/E = 0.05$ )

calculated thermal stress, also known as “secondary stress”, of  $\sigma_T/f_y = 0.9$  and  $2.5$ , respectively, was applied there, associated with a negative sign in the left bar and a positive sign in the right bar.

These results were, as were many others in this book, achieved with the finite element program ANSYS [5]. It should be noted that linear and multilinear kinematic hardening is implemented in the KINH material model on the basis of [6], leading to incorrect results in the case of plane stress when adopting the element types PLANE182 or PLANE183. This manifests itself by unequal strains in the two transverse directions with a uniaxial stress state.<sup>2</sup> For all other element types the correct results are obtained with the KINH model, but under plane stress conditions only with the legacy element types PLANE42 or PLANE82, or by using the BKIN material model for linear kinematic hardening. For more details see Chap. 6.

<sup>2</sup>Ansyes Inc. says: “Regarding defect #92325, this is not a defect but a limitation with the sublayer/overlay model according to development”.

The smaller thermal stress (Fig. 2.5) leads to elastic shakedown after theoretically an infinite number of cycles. After about 35 cycles, however, the strain increments per cycle are so small that the shakedown process can be considered virtually complete. The second parameter combination (Fig. 2.6) leads to plastic shakedown after eight cycles. It can be concluded from the stress–strain diagram, by the way, that the same (elastic shakedown) or almost the same (plastic shakedown) level of strain would be reached for isotropic hardening, as reversed plastic straining does not happen at all or, if so, only to a minor degree.

## 2.4 Ratcheting Interaction Diagram

The stress levels, which result in elastic or plastic shakedown or ratcheting, can be depicted for a given system of component geometry and loading conditions in a so-called ratcheting interaction diagram (RID), sometimes also called a shakedown map. This is shown in Fig. 2.7 for the two-bar model with constant primary and cyclic thermal stress for a linear elastic-perfectly plastic as well as for a linear kinematic hardening material as treated in Sects. 2.2 and 2.3. Because of the pulsating character of the loading (Fig. 2.3), the linear elastic calculated secondary stress  $\sigma_t$  not only marks the maximum value of the stress produced by the thermal load but is also identical to the stress range.

A normalized primary stress  $\sigma_P/f_y > 1$  is not possible with non-hardening material, because then the plastic limit load would be exceeded. Although the plastic limit load is defined only for perfectly plastic material, its exceedance is not tolerated in practice even for a hardening material, although the system would then still not be kinematic.

For sufficiently small values of pairs of primary and thermal stress, the structure remains purely elastic (region E). Without hardening (Fig. 2.7, left) the area of plastic shakedown (region PS) degenerates to a line at  $\sigma_P/f_y = 0$  and  $\sigma_t/f_y > 2$  in this

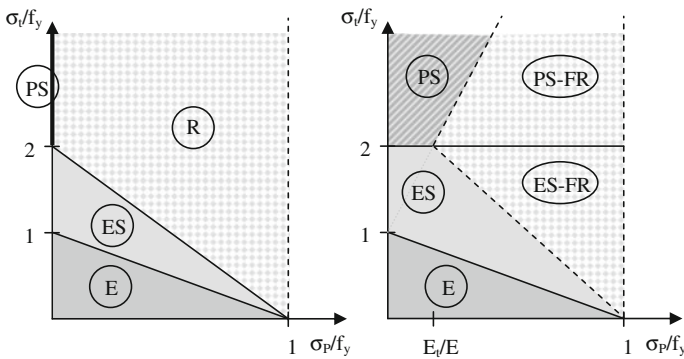


**Fig. 2.7** Ratcheting interaction diagram for the two-bar model; *left* with linear elastic-perfectly plastic material; *right* with linear kinematic hardening



example. Later we get to know examples where the region PS can also cover an area despite the lack of hardening. Ratcheting (region R) is only possible in the presence of a primary stress in this example ( $\sigma_P/f_y > 0$ ). An example is shown in Sect. 2.5.1 in which ratcheting occurs even without primary stress. The region ES indicates elastic shakedown.

With unlimited hardening, ratcheting is not possible in the sense of infinitely large strains after infinitely many load cycles. As already mentioned, there is instead guaranteed shakedown, so it comes to limited strains after an infinite number of load cycles. The RID now provides only a qualitative statement about the nature of shakedown.

With kinematic hardening, plastic shakedown is obtained if the elastically calculated range of the thermal stress exceeds twice the yield stress, and elastic shakedown if it falls below twice the yield stress. A quantitative statement about the level of strain, which is connected with the respective state of shakedown, cannot be directly derived from the RID. However, the regions ES and PS can be further subdivided to differentiate certain types of behavior of the structure. In particular, we may be interested in the identification of regions in which shakedown is not achieved within only one loading cycle, but where strains are accumulated over several or many or even an infinite number of cycles, so that larger strains may develop. For such regions, Mulcahy [2] has already used the term “finite ratcheting” (FR). Thus, Fig. 2.7 (right) has regions PS-FR and ES-FR in which finite ratcheting leads to plastic or elastic shakedown. In the case of unlimited isotropic hardening, only the regions E, ES, and ES-FR can exist.

Figure 2.7 shows clearly that ratcheting can occur even at low ranges of loading and therefore in “predominantly” static loading—i.e., without necessarily being linked to an LCF problem.

---

## 2.5 Examples of Ratcheting

In the next sections, examples of other configurations of component geometry and load type are treated, allowing insights into the occurrence of ratcheting.

### 2.5.1 Three-Bar Model

A third bar is added to the two-bar model considered in the previous sections (Fig. 2.8). The thermal stress is no longer applied only in one bar, but one after the other in all three bars, so that unsymmetrical behavior occurs.

This configuration can be viewed as a simple model for a pulsating thermal load on the inner surface of a (pipe) wall and consequently temperature peaks traveling through the wall. The two-bar model treated in the previous sections could, however, at most be regarded as a simple model for a wall with blockwise distributed

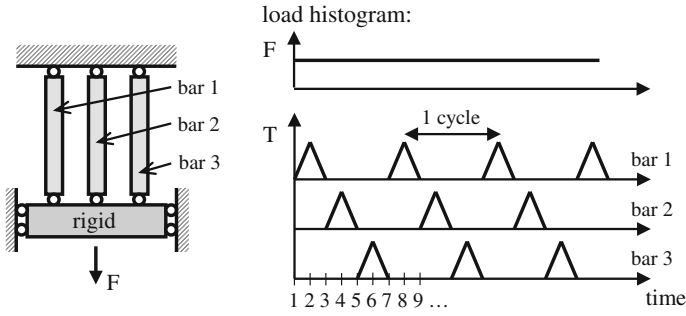
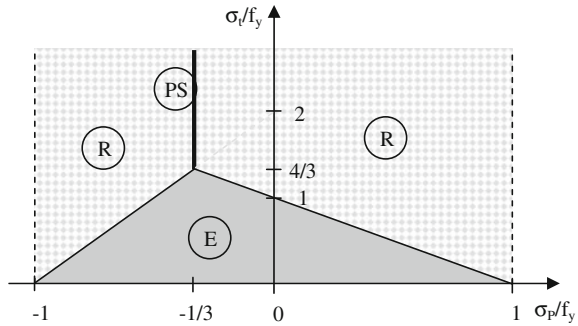


**Fig. 2.8** Three-bar model

**Fig. 2.9** Ratcheting interaction diagram for the three-bar model



temperatures occurring cyclically. A different configuration of a three-bar model has already been examined by Wolters and Majumdar in [7].

At a time of loading in which one bar is at maximum temperature, causing a linear elastic calculated thermal stress  $\sigma_t$ , the other two bars are stressed by  $-\sigma_t/2$ . Accordingly, the linear elastic stress range of the thermal stress is  $\Delta\sigma_t = 1.5 \sigma_t$ .

Figure 2.9 shows the corresponding ratcheting interaction diagram for the three-bar model for linear elastic-perfectly plastic material.

As with the two-bar model the region of plastic shakedown is degenerated to a line for a non-hardening material. However, there are some other remarkable features:

- There is no region of elastic shakedown
- The RID is not symmetrical with respect to the primary stress
- Even in the absence of a primary stress ( $\sigma_p = 0$ ), a ratcheting mechanism is developing as soon as plastic straining is caused by the thermal load
- Even if the bars are under compression produced by the constant external force  $F$ , ratcheting may occur in tension, namely for  $\sigma_p/f_y > -1/3$ .

## 2.5.2 Multiaxial Ratcheting

### 2.5.2.1 Tube Under Internal Pressure and Displacement-Controlled Elongation

So far, structural ratcheting has been represented only in uniaxial stress states. Now a thin-walled tube under constant internal pressure and cyclic heating is considered, where thermal expansion in the longitudinal direction is prevented. The circumferential membrane stresses are then stress-controlled and the axial membrane strains are strain-controlled. At least at a sufficient distance from the ends of the tube there is a biaxial homogeneous state of stress, which can be studied in an isolated material point or at a single finite element: In one direction a constant force  $F$  acts, causing the primary stress  $\sigma_P$ , and orthogonal thereto a cyclic strain (Fig. 2.10). Because of the homogeneity of the stress state, this case was categorized under material ratcheting in [8].

With unit lengths chosen as dimensions in Fig. 2.10, the force  $F$  causes a biaxial primary stress condition with the Mises equivalent stress

$$\sigma_P = \sqrt{1 - \nu + \nu^2} F. \quad (2.6)$$

The elastic limit load is reached at  $\sigma_P = f_y$ . If the (elastic) Poisson's ratio  $\nu = 0$ , the force  $F$  causes only a uniaxial primary stress  $\sigma_P$  in coordinate direction (1).

The displacement  $u$  generates stresses only in coordinate direction (2). For a non-hardening material the yield surface is immutable. At sufficiently high load, a plastic strain increment arises in each extreme value of the cyclic loading that is directed perpendicular to the Mises circle at the position vector of the respective stress state because of the normality rule (see Figs. 1.4 and 1.6). The component of the plastic strain, which acts in the coordinate direction (2) is exactly opposite at the two extreme values of the cyclic loading and is thus cancelled out over an entire load cycle. The component perpendicular to this is, however, equally directed at the two extreme values of the cyclic loading and thus adds up over a whole load cycle, so that each load cycle is creating a net strain increment (Fig. 2.11). This acts in the direction of coordinate (1), as well as with the same intensity but opposite sign in the direction of coordinate (3).

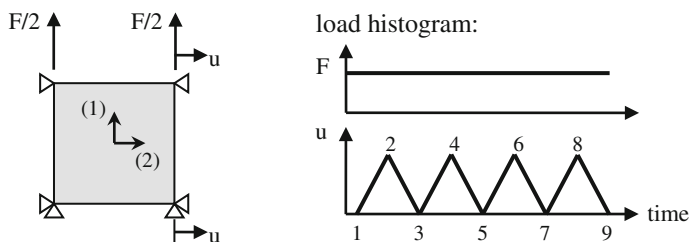
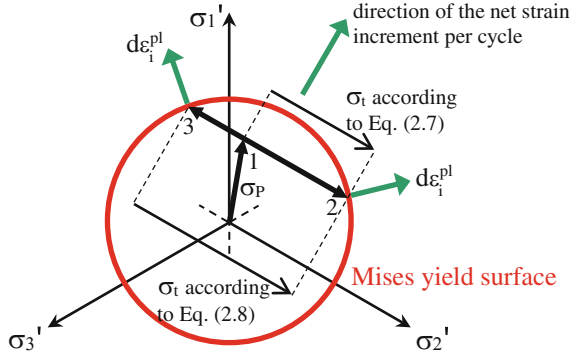


**Fig. 2.10** Multiaxial ratcheting: replacement model for a thin-walled tube under internal pressure and displacement-controlled change of length

**Fig. 2.11** Multiaxial ratcheting with linear elastic-perfectly plastic material: deviatoric stress space



The displacement-controlled load generates the elastic calculated  $\sigma_t$ . The elastic limit load is reached at

$$\frac{\sigma_t}{f_y} = \frac{\left(\frac{1}{2} - \nu\right) \frac{\sigma_P}{f_y} \pm \sqrt{\left(1 - \nu + \nu^2\right) - \frac{3}{4} \left(\frac{\sigma_P}{f_y}\right)^2}}{\sqrt{1 - \nu + \nu^2}}. \quad (2.7)$$

If this is exceeded, plastic straining is initiated and the stress vector in Fig. 2.11 does not return from point 2 to point 1 in the subsequent unloading half cycle, but overshoots it. If the displacement-controlled load is not too large, so that the yield point is not reached again at time 3, only purely elastic behavior takes place during the following load cycles. After just one load cycle, elastic shakedown (ES) is achieved (Fig. 2.11).

At sufficiently large displacement-controlled load, the yield surface is again reached at time 3, associated with further plastic action. Thus, the limit state of elastic shakedown is reached. As no directional redistribution can take place in the present system, and no region of plastic shakedown can exist here with linear elastic-perfectly plastic material, the ratcheting limit is reached at

$$\frac{\sigma_t}{f_y} = \sqrt{4 - \frac{3}{(1 - \nu + \nu^2)} \left(\frac{\sigma_P}{f_y}\right)^2}. \quad (2.8)$$

Equations (2.7) and (2.8) are depicted in Figs. 2.12 and 2.13 for  $\nu = 0$  and  $\nu = 0.5$ , respectively.

With linear kinematic hardening, infinite ratcheting is not possible, but either elastic or plastic shakedown is guaranteed. However, it is difficult to identify the boundaries between the regions of ES and ES-FR (elastic shakedown after more than one cycle) or between PS and PS-FR (plastic shakedown after more than one cycle). For this, incremental analysis would be needed, which are discussed later, because the normal direction is constantly changing during the loading process. In addition, the result would be dependent not only on the range of the loading

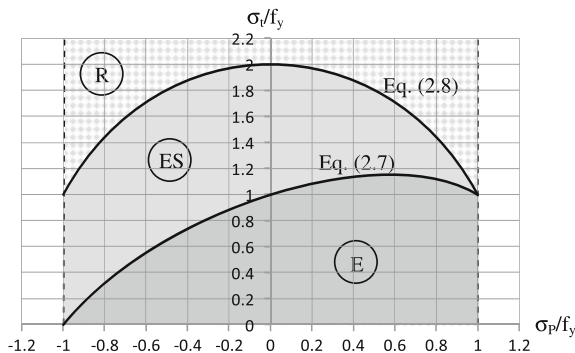
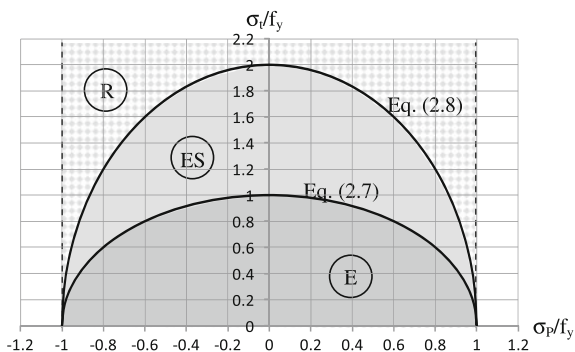


**Fig. 2.12** RID for multiaxial ratcheting with linear elastic-perfectly plastic material and  $\nu = 0$

**Fig. 2.13** RID for multiaxial ratcheting with linear elastic-perfectly plastic material and  $\nu = 0.5$



intensity but also on whether the displacement-controlled load is applied swelling as shown in the load histogram of Fig. 2.10 or unequal to zero at minimum load level. Therefore this distinction is omitted in the RID (Fig. 2.14), and is largely omitted in the rest of this book.

The border between ES and PS is given solely by the range of the displacement-controlled load:

$$\frac{\sigma_t}{f_y} = 2. \quad (2.9)$$

If the elastically calculated stress range exceeds twice the yield stress, PS occurs as already noted in the two-bar model (Fig. 2.7). In the present case, this is explained by the fact that the Mises yield surface gradually shifts with the number of cycles in the deviatoric stress space until the cyclically varying stress passes through the centers of the two Mises circles belonging to the extreme loading conditions (marked by crosses in Fig. 2.15). For subsequent cycle numbers  $n$ , the system behaves periodically. At loading times  $1 + n$  and  $2 + n$  the normals to the

**Fig. 2.14** RID for multiaxial ratcheting with linear kinematic hardening material and  $\nu = 0$

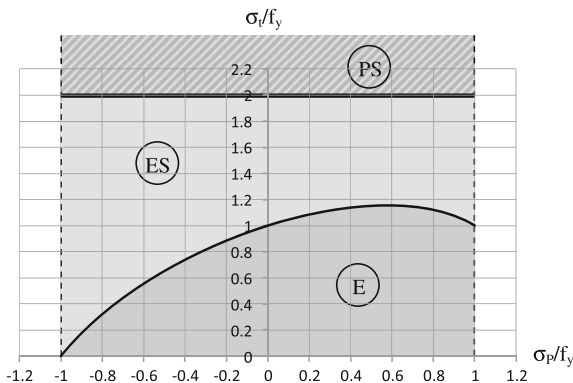
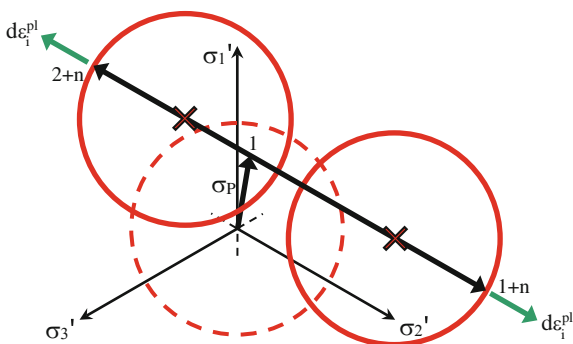


**Fig. 2.15** Multiaxial ratcheting with linear kinematic hardening material: PS in the deviatoric stress space



yield surfaces and thus the plastic strain increments are directly opposite, so that they cancel each other out over two consecutive half cycles.

The distance between the two Mises circles can be determined easily in the state of shakedown from the elastic-plastic strain applied as loading and the hardening law (see Eq. (1.26)). However, this does not automatically apply to the position of the Mises circles and thus not to the strain accumulated by finite ratcheting, because the normal direction constantly changes during the loading process with the load level, so that an incremental analysis is necessary.

In the case of elastic shakedown, the Mises yield surface is shifted as shown in Fig. 2.16, until the length of the circle chord corresponds to the elastically calculated stress range. During subsequent cycle numbers,  $n$ , their position is fixed. However, this position of the yield surface and thus the strain accumulated by finite ratcheting are only determinable with an incremental analysis.

In Fig. 2.17 the development of plastic strain components over the number of half cycles as derived from an incremental analysis is shown as an example of a loading configuration leading to ratcheting with a non-hardening material, but leading to elastic shakedown with linear kinematic hardening.

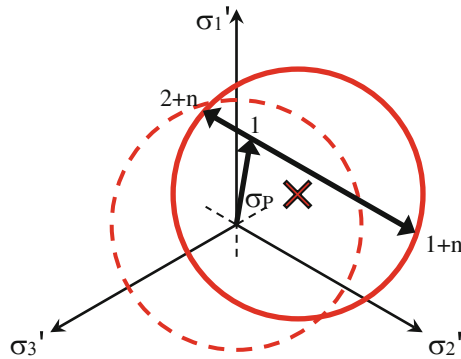


**Fig. 2.16** Multiaxial ratcheting with linear kinematic hardening material: ES in the deviatoric stress space

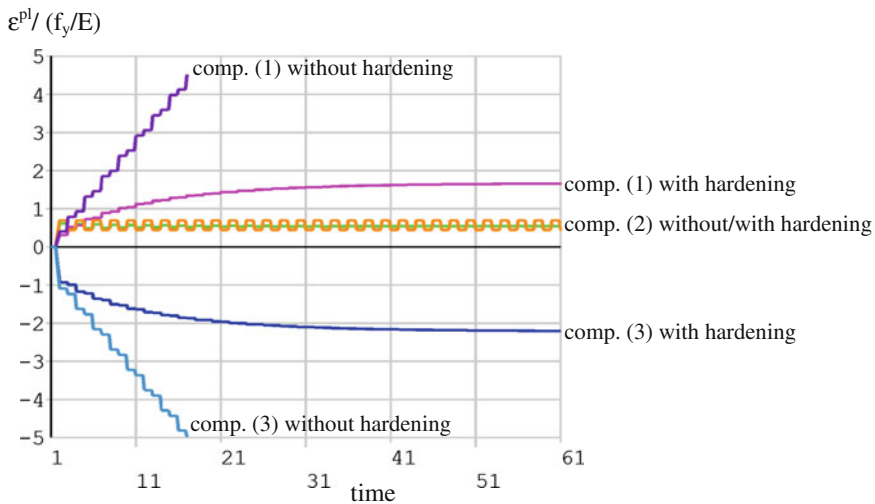


**Fig. 2.17** Multiaxial ratcheting: histogram of plastic strains ( $\sigma_P/f_y = 0.8$ ;  $\sigma_d/f_y = 1.5$ ;  $E_d/E = 0$  and  $0.05$ ;  $\nu = 0.3$ )

### 2.5.2.2 Tube Under Axial Force and Displacement-Controlled Twist

A situation similar to that for the thin-walled tube with constant internal pressure and cyclic displacement-controlled change in length, and its replacement model shown in Fig. 2.10, is also encountered in a thin-walled tube being pulled in a longitudinal direction with a constant force and being displacement-controlled cyclically twisted (Fig. 2.18)—a situation that has been used several times for ratcheting experiments. This can be simplified to a single material point under constant uniaxial normal stress  $\sigma$  and cyclic distortion  $\gamma$ , causing shear stresses  $\tau$ .

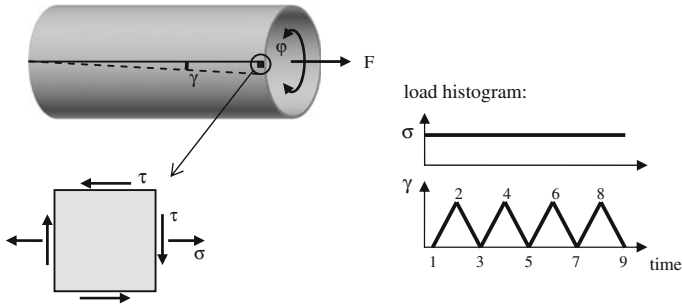
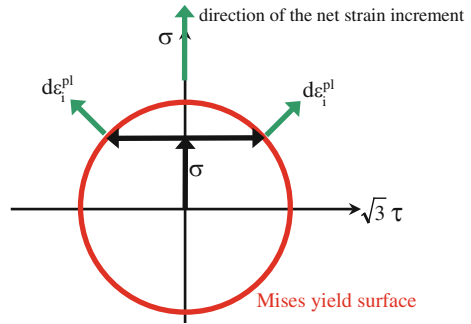


**Fig. 2.18** Multiaxial ratcheting: thin-walled tube under axial force and displacement-controlled twist

**Fig. 2.19** Multiaxial ratcheting with linear elastic-perfectly plastic material for the system in Fig. 2.18



A representation of the stress path in the space of the principal deviatoric stresses is not possible because the principal stress directions do not remain constant during the loading process. Instead, it can be represented in the  $\sigma - \sqrt{3}\tau$ -plane, where the Mises yield condition

$$f_y = \sqrt{\sigma^2 + 3\tau^2} \quad (2.10)$$

appears as a circle (Fig. 2.19). It can be deduced easily that the RID for non-hardening material is identical with Fig. 2.13 if  $\sigma_p$  is replaced by  $\sigma$  and the  $\sqrt{3}$ -fold elastically calculated shear stress  $\tau$  is set in place of  $\sigma_r$ . Accordingly, the boundaries between the regions E, ES, and R are given by Eqs. (2.7) and (2.8) if  $\nu = 0.5$  is used.

### 2.5.3 Bree Tube

The Bree tube is probably the best known example of ratcheting. For some decades it has represented the basis for design rules against ratcheting in many standards, for example, in German nuclear codes [9].



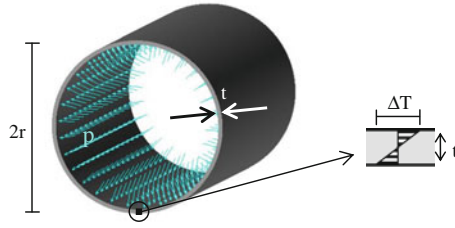


**Fig. 2.20** Bree tube with open ends; temperature distribution over the wall thickness

A thin-walled tube (radius  $r$ , wall thickness  $t$ ) is subjected to a constant internal pressure  $p$  (Fig. 2.20). This produces the axisymmetric stresses

$$\sigma_p = \begin{cases} \frac{pr}{t} & \text{in circumferential direction} \\ \frac{pr}{2t} & \text{in axial direction} \\ \approx 0 & \text{in radial direction} \end{cases} \quad (2.11)$$

The axial stress is attributed to the force which acts on the end surfaces of a closed tube. It vanishes, if the tube is to be regarded as open. The stresses only apply at sufficient distances from the ends of the tube (principle of St. Venant). Because of the thin walls, they are membrane stresses, solely attributable to equilibrium requirements and are thus independent of the material behavior.

If a liquid medium moving through the tube changes its temperature, then a temperature distribution is produced through the wall, which is approximately linear in the stationary state because of the thin walls, provided that the outside surface is not insulated but the temperature is kept constant there. The membrane fraction of the thermal expansion strain can develop freely if the tube is supported without axial constraint. However, the temperature difference  $\Delta T$  between the outer and inner surfaces causes thermal expansion strains that result in equal but oppositely directed mechanical bending strains, because the pipe cannot perform bending deformation across the wall thickness. These bending strains are of equal size in the circumferential and axial directions and are distributed axisymmetrically. For linear elastic material, or fictitiously calculated elastic material, the stresses at the two surfaces become

$$\sigma_t = \begin{cases} \pm \frac{E}{2(1-\nu)} \alpha_t \Delta T & \text{in circumferential direction} \\ \pm \frac{E}{2(1-\nu)} \alpha_t \Delta T & \text{in axial direction} \\ \approx 0 & \text{in radial direction} \end{cases} \quad (2.12)$$

Miller [1] and, later, Bree [10] have approximated the biaxial stress state caused by internal pressure and radial temperature gradient by a uniaxial stress state as in a flat sheet metal strip, which corresponds to the circumferential direction of the tube. Miller has already pointed out that even Hill [11] examined the steady decrease of the wall thickness of a plate under cyclic bending.

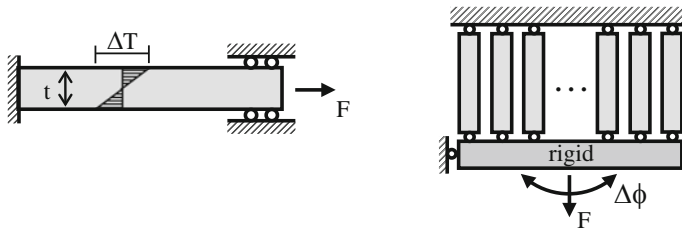


**Fig. 2.21** Replacement models with uniaxial state of stress for the Bree tube; *left* beam with linear temperature distribution; *right* coupled rods with displacement-controlled rotation

For this purpose, a beam of height  $t$  is supported at both ends against rotation and lateral displacement, but only at one end against axial displacement (Fig. 2.21). At the other end, a constant axial force  $F$  is applied. Across the height of the beam a linear temperature distribution with the difference  $\Delta T$  is applied cyclically. Because this is constant in the axial direction, the length of the beam does not matter. Therefore, it is also sufficient, to replace the beam height  $t$  by infinitely many parallel rods, coupled by a rigid plate to satisfy the first Bernoulli hypothesis, stating that plane sections remain plane, and loaded by a cyclic displacement-controlled rotation instead of the thermal loading of the beam (Fig. 2.21).

If restricted to two instead of an infinite number of rods, we get ultimately the two-bar model treated in Sect. 2.2.

Bree first completed the RID for the uniaxial replacement model of the Bree tube subjected to pulsating thermal loads for linear elastic-perfectly plastic material on the basis of the results obtained by Miller, before extending it with regard to linear kinematic hardening material. The corresponding RID (Fig. 2.22) is simply referred to as the Bree diagram. It is often, especially in English language literature, down-right eponymous for ratcheting interaction diagrams at all (Bree-like diagrams).

The boundary between plastic shakedown and ratcheting for linear elastic-perfectly plastic material is given by the hyperbola

$$\frac{\sigma_t}{f_y} = \frac{1}{\frac{\sigma_P}{f_y}} \geq 2 \quad (2.13)$$

and for linear kinematic hardening by

$$\frac{\sigma_t}{f_y} = \frac{1 - \frac{E_t}{E}}{\frac{\sigma_P}{f_y} - \frac{E_t}{E}} \geq 2. \quad (2.14)$$

The Bree diagram has been very intensively studied in the literature, for example in terms of its appropriateness to represent the actually biaxial stress state in the original Bree tube, in terms of the difference between an open and a closed tube, in terms of alternating instead of swelling thermal load, with regard to cyclic primary stress either in or out of phase with the cyclic temperature, and in terms of

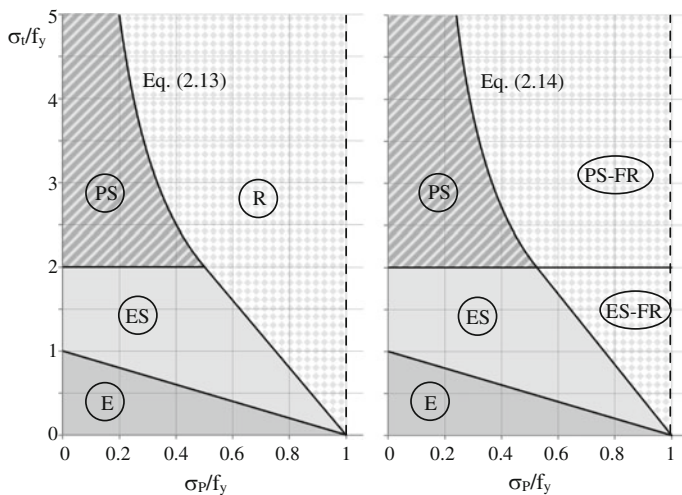


**Fig. 2.22** Bree diagram; *left* linear elastic-perfectly plastic material; *right* linear kinematic hardening material ( $E_p/E = 0.05$ )

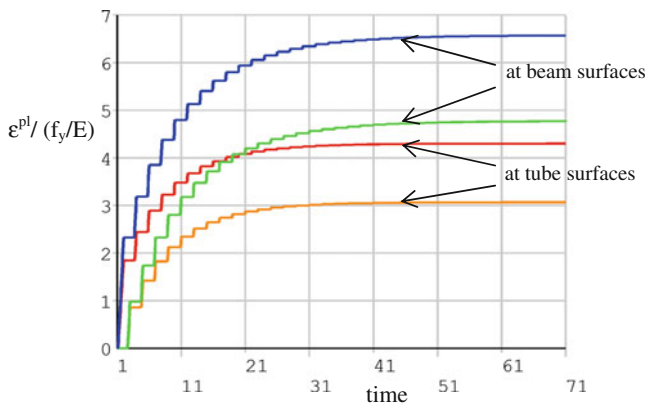


**Fig. 2.23** Plastic strain histogram at each of the two surfaces in ES ( $\sigma_p/f_y = 0.8$ ;  $\sigma_t/f_y = 1.9$ ;  $E_p/E = 0.05$ ): Bree tube (multiaxial stress state,  $\nu = 0.3$ , circumferential component) and replacement beam with uniaxial stress state

additional stresses from piping forces. Solutions for parabolic [1] or bilinear [12] instead of linear temperature distribution over the wall thickness have also found their way into the regulatory framework (such as [9]).

For a configuration of loading parameters in region ES-FR, Fig. 2.23 indicates exemplarily that the replacement beam investigated by Bree (Fig. 2.21) is a conservative simplification of the original tube (Fig. 2.20) with respect to the plastic strains. The same maximum secondary stress was chosen for both models ( $\sigma_t = 1.9 f_y$ ), for which a lower temperature gradient had to be applied at the tube than at the beam:

$$\Delta T_{\text{tube}} = 2\sigma_t \frac{1 - \nu}{E\alpha_t} \quad (2.15)$$

$$\Delta T_{\text{beam}} = 2\sigma_t \frac{1}{E\alpha_t} . \quad (2.16)$$

## 2.5.4 Continuous Beam

So far, the ratcheting behavior of structures that are subjected to thermal or other displacement-controlled loadings such as displacements of supports has been discussed. Now, a structure is considered which is subjected to a force-controlled load only and Burth and Brocks [13] have already dealt with it in detail: A continuous beam of two equally long fields is loaded in the middle of the first field by a constant force  $F_1$  and in the middle of the second field by a cyclically pulsating force  $F_2$  ( $F_2 = 0$  to  $F_1$ ) (Fig. 2.24).

Only bending is considered, so that shear deformation produced by the lateral forces is disregarded. To understand the ratcheting process it is sufficient to make use of the plastic hinge theory, according to which plastic straining is confined to discrete sections. The cross-section behaves linearly elastic below the plastic moment  $M_{pl}$ , and after the plastic hinge is developed, the section cannot carry a moment higher than  $M_{pl}$ . This behavior corresponds to a linear elastic-perfectly plastic material, but not in terms of stress and strain, but in terms of generalized stress and strain, i.e., for a moment–curvature relationship.

At time 1, only the force  $F_1$  is active. Its value is chosen so that the plastic moment is exceeded by 12 % at location 1 if the theory of elasticity is applied (which is the case with  $F = 2.5 M_{pl}/L$ ), so that a plastic hinge is produced there, in which the full plastic moment is acting (Fig. 2.25).

Accordingly, a plastic kink  $\varphi_{1(t1)}$  is created at location 1. At time 2 an additional second force  $F_2$  (same intensity as  $F_1$ ) is applied in the second field. This causes the plastic hinge at the location 1 to be relieved, so that although the kink  $\varphi_{1(t1)}$  is maintained and acting as a constraining load, the moment is reduced there. Simultaneously, a new plastic hinge is formed at the inner support so that the plastic moment  $M_{pl}$  is acting there with a negative sign, associated with a plastic kink  $\varphi_{s(t2)}$ .

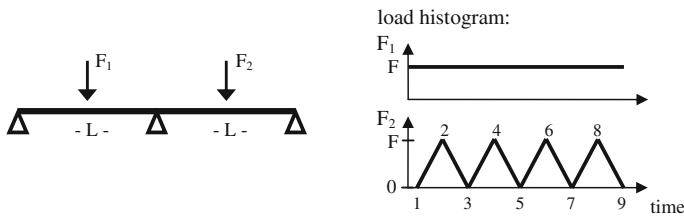


**Fig. 2.24** Continuous beam

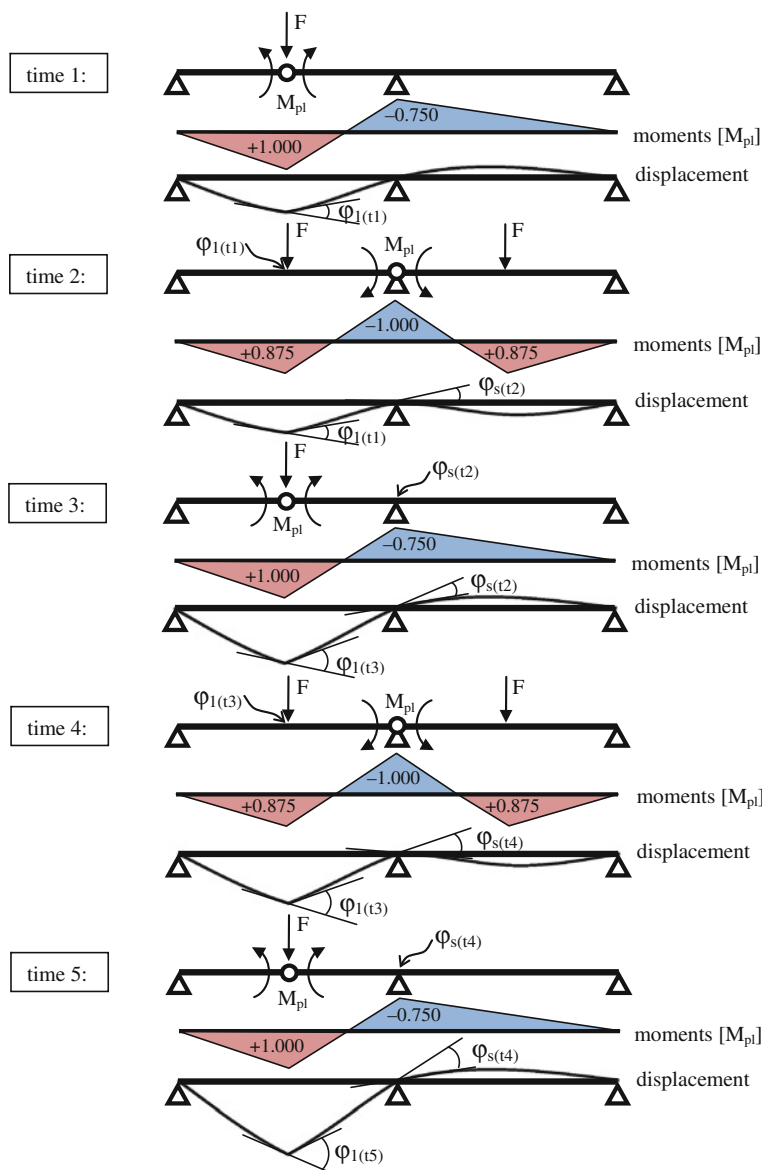


**Fig. 2.25** Ratcheting of the continuous beam

If at time 3 the force  $F_2$  is now removed, the plastic hinge is relieved at the inner support, but the plastic kink  $\phi_{s(t2)}$  is retained there, so only the magnitude of the moment decreases. Instead, the moment grows at the position of force  $F_1$  until the plastic moment is again reached, so again the plastic hinge is activated with a

corresponding plastic kink  $\varphi_{1(t3)}$ . The structural system is now the same as at time 1, but an additional constraining load is introduced in terms of kink  $\varphi_{s(t2)}$ . Because it is a statically determinate system because of the plastic hinge, this constraining load causes no internal forces, but merely deformation. The moments are equally distributed at times 1 and 3, although the displacements are not!

Upon renewed application of force  $F_2$  at time 4, and maintaining the kink  $\varphi_{1(t3)}$  at location 1, the moment at the inner support increases in magnitude again until again the plastic moment is reached and the plastic kink  $\varphi_{s(t4)}$  is formed, whereas at location 1 the moment decreases. The structural system and the moments are now therefore the same as at time 2, but the constraining load at location 1 has changed and, consequently, the displacements as well. Accordingly, the kink in the plastic hinge is now different from the time 2 ( $\varphi_{s(t4)} \neq \varphi_{s(t2)}$ ).

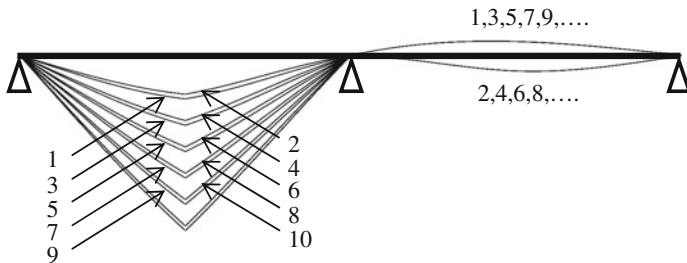
Thus another starting point exists for the following removal of the load  $F_2$  (time 5) as for the removal of the load at time 3. Accordingly, the displacements at time 5 and also the plastic kink at location 1 differ from those at time 3.

In turn, the displacements at time 6 are different than at time 4, at time 7 different than at time 5, etc. After each load cycle only the displacements are different in the present case, although the magnitudes of the moments are always the same. The change of displacements is equal in each cycle, so that the deflections in the left field increase linearly with the number of cycles (Fig. 2.26).

In Fig. 2.27 the histogram of the bending moments at the two positions of the plastic hinge is shown for the first five cycles. So it is easy to see that there is no alternating plasticity and thus there is no pronounced fatigue problem.

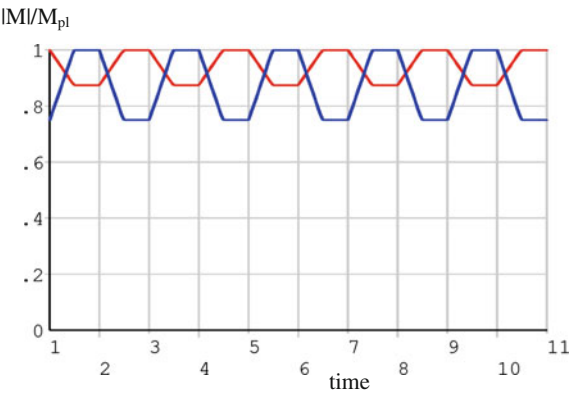
Ratcheting arises here because two plastic hinges are alternately active. It is worth noting that the applied load is only force-controlled. However, because of the static indeterminacy of the system, constraints are present which have displacement-controlled character.

Figure 2.28 shows the RID for the loading configuration of constant force  $F_1$  and pulsating force  $F_2$ . The axes are scaled to the plastic limit loads  $F_{1T}$  and  $F_{2T}$ , obtained for the sole effect of  $F_1 = F$  or  $F_2 = F$ , respectively. Three different regions of elastic shakedown are recognizable, depending on whether a plastic hinge is formed at one of the two locations of the applied forces or at the inner

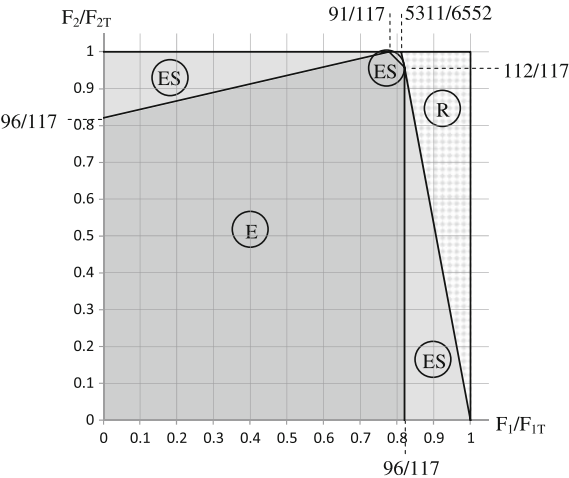


**Fig. 2.26** Displacements of the continuous beam at different times because of ratcheting

**Fig. 2.27** Histogram of the bending moments at the plastic hinges of the continuous beam (*red* in the middle of the left field, *blue* at the support)



**Fig. 2.28** RID of continuous beam with a constant force  $F_1$  and cyclic force  $F_2$  (both axes scaled by the respective plastic limit loads for  $F_1$  and  $F_2 = F$  alone)



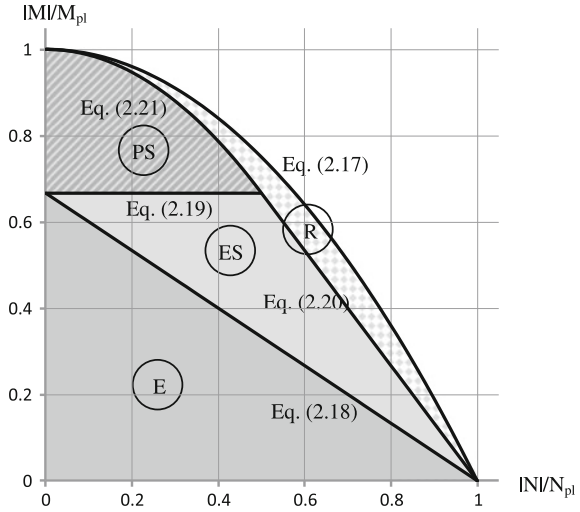
support (the small triangle at the top of RID). A region of plastic shakedown does not exist. The elastic limit refers here to the advent of a plastic hinge in a section, not to incipient plastic straining in one of the outermost fibers of a section. Possibilities and limits of plastic system reserves are hereby demonstrated for this configuration of a two-field beam.

### 2.5.5 Interaction of Section Forces

In the previous section, plastic system reserves were the subject of consideration, but a look is now taken at plastic cross-section reserves.

Because the boundary between elastic or plastic shakedown on the one hand and ratcheting on the other is always reached at load levels below the plastic limit load with linear elastic-perfectly plastic material behavior, the plastic capacity of a

**Fig. 2.29** Bearing capacity of a rectangular cross-section: RID of constant normal force and alternating bending moment



cross-section is decreased in the presence of even slightly varying load, as almost always present. The capacities of cross-sections derived for monotonic loading should therefore not be exploited, or you should at least be aware that existing safety margins are partly depleted for this.

As an example, a solid rectangular cross-section under force-controlled loading by a constant normal force and an alternating bending moment is considered. In [14] and [15] the RID is given for a linear elastic-perfectly plastic material (Fig. 2.29).

The plastic limit load under monotonic loading is given by

$$\frac{|M|}{M_{pl}} + \left(\frac{N}{N_{pl}}\right)^2 = 1 \quad (2.17)$$

and the elastic limit load by

$$\frac{3|M|}{2M_{pl}} + \frac{|N|}{N_{pl}} = 1. \quad (2.18)$$

The region of elastic shakedown is bounded by

$$\frac{3|M|}{2M_{pl}} = 1 \quad \text{for} \quad 0 \leq \frac{|N|}{N_{pl}} \leq 0.5 \quad (2.19)$$

$$\frac{3|M|}{4M_{pl}} + \frac{|N|}{N_{pl}} = 1 \quad \text{for} \quad 0.5 \leq \frac{|N|}{N_{pl}} \leq 1 \quad (2.20)$$



and the region of plastic shakedown by

$$\frac{|M|}{M_{pl}} + \frac{4}{3} \left( \frac{N}{N_{pl}} \right)^2 = 1. \quad (2.21)$$

The origin of Eq. (2.21) depicted in the RID of Fig. 2.29 possibly requires some explanation. For determining the upper boundary of the plastic shakedown region, the relation between normal force or bending moment and membrane strain  $\varepsilon_m$  or bending strain  $\varepsilon_b$  may be expressed by

$$\frac{N}{N_{pl}} = \frac{\varepsilon_m}{\varepsilon_b} \quad (2.22)$$

$$\frac{M}{M_{pl}} = 1 - \frac{1}{3} \left( \frac{f_y/E}{\varepsilon_b} \right)^2 - \left( \frac{\varepsilon_m}{\varepsilon_b} \right)^2. \quad (2.23)$$

Now use is made of the relationship between a constant normal force and displacement-controlled bending as represented by the Bree diagram (Fig. 2.22, left). The boundary between plastic shakedown and ratcheting, Eq. (2.13), can, because  $\sigma_t$  is the linearly elastic calculated bending stress, also be formulated by

$$\frac{\sigma_t}{f_y} = \frac{\varepsilon_b}{f_y/E} = \frac{1}{N/N_{pl}} \geq 2. \quad (2.24)$$

Insertion of Eqs. (2.22) and (2.24) into Eq. (2.23) then yields Eq. (2.21).

Ratcheting takes place in the region between the shakedown states and the limit load, which manifests itself in an increase in the membrane stretching in the direction of the normal force in each load cycle. For a given normal force, the cross-section can only be loaded less for cyclic than for monotonic loading. The reduction is up to one-ninth of the plastic moment (at  $N/N_{pl} = 2/3$ ), or, in other terms, the load bearing capacity of the cross-section is reduced by up to one-third compared to monotonic loading (for  $N/N_{pl} \rightarrow 1$ ).

## 2.6 Myths About Ratcheting

Among working engineers and scientific publications, and even in codes and standards for the design of structures, a number of myths have been disseminated which can be corrected based on the findings in the previous sections.

### ***Myth 1: Ratcheting Only Occurs at Very High Cyclic Loads***

The underlying idea, nourished by design codes, is that ratcheting is a byproduct of LCF (low cycle fatigue: fatigue damage at small numbers of load changes and high strain ranges), and could thus only occur in conjunction with alternating

plasticity, i.e., in terms often used by design codes such as the KTA rules [9] only when  $S_n > 3 S_m$ .

This perception is not true as we can see from the ratcheting-interaction diagrams of the last sections. The two-bar model (Fig. 2.7) shows that ratcheting can occur far below the threshold of cyclic plasticity (i.e., when  $\sigma_i/f_y < 2$ ) if the constant primary stress is large enough.

**Myth 2: In Order For a Ratcheting Mechanism to Develop, a Force-Controlled Load or Primary Stress is Required as a Driving Force, Which Also Must be Present Constantly**

This idea of ratcheting is invalidated through the three-bar model treated in Sect. 2.5.1. The ratcheting interaction diagram (Fig. 2.9) shows that, even without a primary stress (i.e., at  $\sigma_p/f_y = 0$ ), ratcheting may occur.

**Myth 3: In Order to Exclude Structural Ratcheting, all Loads on the Structure Need to be Analyzed only in Pairs**

In fact, the consideration of the extremes of a pair of variable loads is sufficient in many cases to detect or exclude structural ratcheting. This includes the two-bar model ( $F$  alone,  $F + T$  in the left bar), the Bree tube ( $p$  alone,  $p + \Delta T$ ), and the continuous beam ( $F_1$  alone,  $F_1 + F_2$ ). In the three-bar model in Sect. 2.5.1, there are four actions: an external force  $F$  and a temperature peak in each of the three bars. These cause four different loading extremes ( $F$  alone,  $F + T_1$ ,  $F + T_2$ , and  $F + T_3$ ). However, none of the six possible pairs of these four states can constitute a ratcheting mechanism, but only the combined effect of all four states. So, a ratcheting analysis restricted to pairwise consideration of load conditions could not identify ratcheting correctly.

---

## 2.7 Residual Stresses

Under variable loads, the terms “residual stress” and “residual strain” play a major role. Thus, stresses and strains are those which are present in the structure when, after prior plasticizing, all loads are completely removed, assuming purely elastic behavior. So it is not that the point in time is considered where the variable portion of the loading vanishes, but when the structure is completely unloaded, including constant loads. In the absence of any loads, the residual stresses must satisfy self-equilibrium. They are therefore sometimes also referred to as eigenstresses.

A full discharge of all previously applied loads would often actually be associated with reversed plasticity because of the removal of constant loads, even in the case of elastic shakedown. However, this is not considered. Instead, the fictitious elastic stresses and strains are subtracted from the elastic-plastic state, with the consequence that the residual stresses  $\rho$  and the residual strains  $\epsilon^*$  are often pure operands which are not really present in the structure after complete unloading (Fig. 2.30):

$$\rho_i = \sigma_i - \sigma_i^{\text{fel}} \quad (2.25)$$

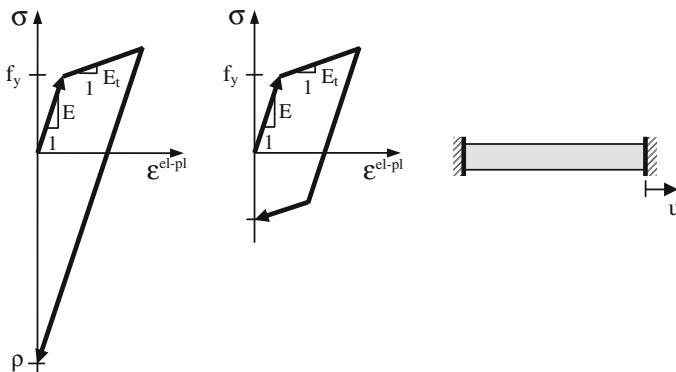


**Fig. 2.30** *Left* residual stress for a tension bar under strain-controlled load with linear kinematic hardening; *right* stress actually remaining after unloading

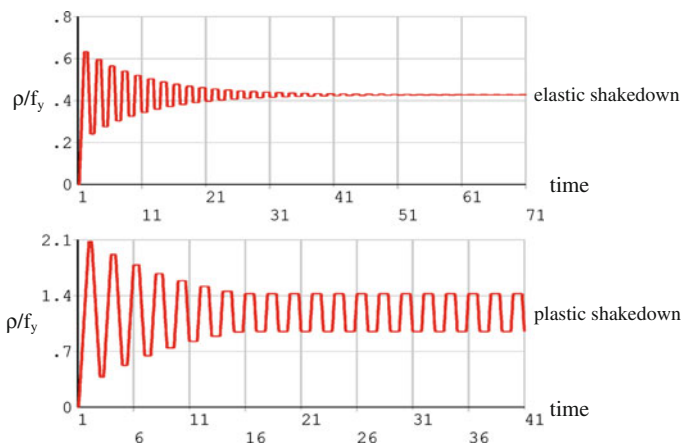


**Fig. 2.31** Histogram of residual stresses for the left bar of the two-bar model with linear kinematic hardening ( $\sigma_p/f_y = 0.8$ ;  $E_t/E = 0.05$ ); *top*  $\sigma_t/f_y = 0.9$ ; *bottom*  $\sigma_t/f_y = 2.5$

$$\varepsilon_i^* = \varepsilon_i - \varepsilon_i^{\text{fel}}. \quad (2.26)$$

The evolution of residual stresses with the number of cycles is shown in Fig. 2.31 for the left bar of the two-bar model with linear kinematic hardening (see Sect. 2.3, Figs. 2.5 and 2.6). It is apparent that the residual stresses remain constant after reaching the state of elastic shakedown.

In Fig. 2.32 the stress–strain hysteresis for both bars is duplicated from Fig. 2.6, supplemented by marking the residual stresses at the time of load reversals in the two bars after the state of plastic shakedown has been reached (squares for times 19, 21, 23, etc., in the load histogram of Fig. 2.3, triangles for times 18, 20, 22, etc.).

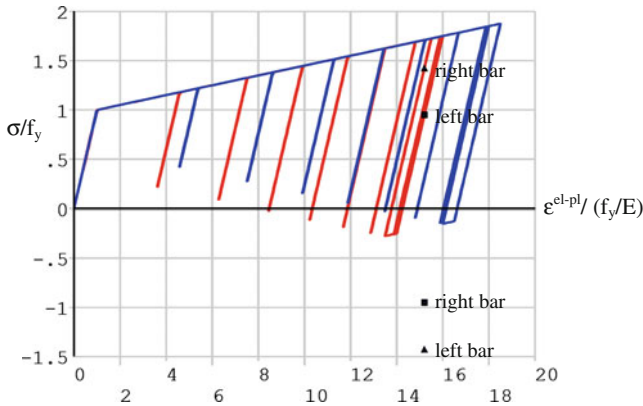


**Fig. 2.32** Stress–strain diagram for the two-bar model as in Fig. 2.6, here complemented with residual stresses and residual strains at load reversals after the plastic shakedown state has been reached

The residual stress states do not apparently necessarily lie on the elastic-plastic material curve. The residual strains are at all times the same in this example after plastic shakedown has been reached, because the thermal load is then strain-controlled with the effect that the plastic strain enhancement factor  $K_e$ , defined as ratio of the elastic-plastic and the fictitiously elastically calculated strain, amounts to  $K_e = 1$ .

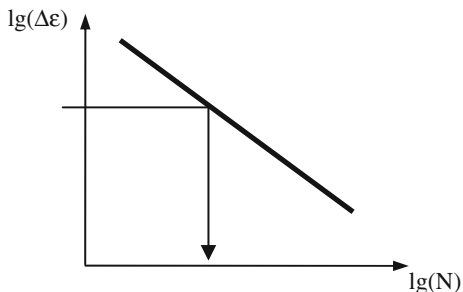
## 2.8 Service Life

### 2.8.1 Fatigue

Sufficient fatigue strength is always to be proven under variable load. There are a number of different concepts, differing in both the way of determining as well as assessing the stresses. Some are based on classical continuum mechanics (nominal stress concept, structure stress concept, local concept), others on fracture mechanics to calculate crack propagation. Some only make use of the elementary strength of materials to determine the stresses without taking account of geometric or metallurgical transitions or locally confined disturbances of the stress pattern at locations of load application. Others require the determination of local stresses with linear elastic or elastic-plastic material laws, usually adopting the finite element method.

Because this book is aimed at determining elastic-plastic stresses and strains, primarily those life proof concepts are of interest here, which can make use of them. This applies to the local concept, which is based on the elastic-plastic strain range used to determine the fatigue usage by means of strain-based fatigue curves (Wöhler curve, SN curve) that have been experimentally determined by uniaxial strain-controlled tests (see, for example, [17]). Here it is essentially to distinguish

**Fig. 2.33** Fatigue curve (schematic)



between the LCF (= low cycle fatigue, i.e. large strain ranges associated with portions of plastic strain; less than 20,000 cycles to failure), the HCF (= high cycle fatigue, less than 2,000,000 cycles to failure), and the endurance regime.

For fatigue analysis the elastic-plastic strain ranges are to be determined for all six different strain components of a load pair (in certain circumstances also the mean strains or mean stresses). For these, the equivalent strain range is formed, for which the number of allowable load cycles  $N$  can be read from the fatigue curve (Fig. 2.33).

The fatigue usage factor  $u$  then results from the number of load cycles  $n$ , either specified or known from in-service monitoring, and must not exceed the value of 1:

$$u = \frac{n}{N} \leq 1. \quad (2.27)$$

If a structure is subjected to different kinds or levels of loading, then several pairs of loading are formed by means of a counting procedure. Here, mostly the rainflow or the reservoir method is used. The number of occurrences of the elastic-plastic strain ranges of each of these pairs of loadings generates a partial usage factor from the fatigue curve. This in turn is summed up over all load pairs  $i$  according to the linear fatigue accumulation rule by Palmgren-Miner:

$$u = \sum_i \left( \frac{n}{N} \right)_i \leq 1. \quad (2.28)$$

### 2.8.2 Strain Accumulation

The life of a cyclically loaded structure operated in the elastic-plastic regime depends not only on the fatigue phenomenon but also on the phenomenon of ratcheting. Furthermore, the service life of a structure can be limited by other phenomena such as corrosion, wear as a result of contact friction, etc., which, however, are not considered here. Because of the one-way increase in strain and displacement per cycle, ratcheting is primarily associated with the risk of incremental collapse after an infinite number of cycles. This is an ideal imagination,

similar to that of an instantaneous collapse by exceeding the plastic limit load, which is based on assumptions that are no longer met in the state of collapse, such as perfectly plastic material, small strains, and small displacements. In addition, the distortion may become so great in an active ratcheting mechanism, even at a finite number of load cycles, that failure occurs by exceeding the ductility of the material. Also, the serviceability of the structure may have already been lost because of excessive displacements.

As an indirect consequence of ratcheting, cross-sections might be so weakened after a certain number of cycles that the plastic limit load is exceeded, or a stable equilibrium state is no longer possible. Although ratcheting and fatigue are different phenomena, and ratcheting can also occur without significant fatigue, an interaction between the two is also possible. So the strain may alternate around a mean strain or mean stress enlarged by ratcheting with the consequence that the fatigue usage is increased, or the range of applicability of the fatigue curve may be exceeded because of excessive strains.

For this reason, in some regulations, such as the nuclear part of the ASME code, which serves as a basis for many standards worldwide (also [9]), proof is required that certain strain limits are not exceeded at the end of life. This differs depending on the proof format, i.e., whether the strains are determined by simplified or detailed elastic-plastic analyses. They also depend on the distribution of strains across the cross-section. So, different strain limits apply to membrane, linearized, and peak strains. Furthermore, the position of the point under consideration in the structure plays a role, depending on whether it is located in the base material or in a welded joint. Accordingly, the strain limits vary between 0.5 % for the membrane strain in welded joints and 5.0 % for the peak strains in the base material.

For example, in the German KTA safety standards [9] for components of the primary circuit of light water reactors, Sect. 17.13.2 “Simplified check with approximate formulas” under 7.13.2.3 “Proof by limiting strains” requires:

“(5) The sum of all strain increments may not exceed 2 % at the end of life”

or Sect. 17.13.3 “General proof by elastic-plastic analysis” requires:

“(3) The locally accumulated plastic tensile principal strain must not exceed to end of life at any point of a cross-section the following maximum values: 5.0 % in the base material, 2.5 % in welds.”

At this point, it should be noted that ratcheting and fatigue proofs are always required if a variable load is present. In the respectively applicable design codes, the procedure for the fatigue assessment is usually described and for the proof against ratcheting usually not. Sometimes a ratcheting proof is required in design codes only if certain stress ranges are exceeded ( $S_n > 3S_m$ ) and is thus coupled with the need for fatigue analyses, which is, however, theoretically not justified (see Sect. 2.6, Myth 1).

If the proof against ratcheting is performed by limiting the strains, the strain components accumulated through the load cycles at the end of the service life of the

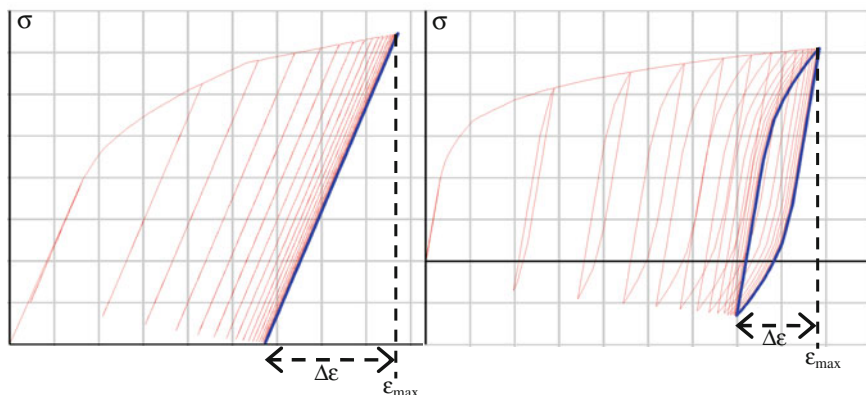


**Fig. 2.34** Elastic-plastic strains required for proof of life; *left* elastic shakedown; *right* plastic shakedown; the cycle of shakedown is highlighted

structure are to be calculated; see the schematic diagram of Fig. 2.34 in a uniaxial stress state. In the state of elastic shakedown (Fig. 2.34, left) the accumulated strain  $\epsilon_{\max}$  is often decisive for the service life, because the strain range  $\Delta\epsilon$  is relatively small. In the state of plastic shakedown (Fig. 2.34, right) either the accumulated strain or the strain range may be life-determining.

It is not sufficient, as a substitute for limiting strains, to prove that the structure for a given load configuration shakes down, and not even that it shakes down elastically (regions ES or ES-FR in the ratcheting interaction diagram), because the state of shakedown may be associated with excessive strains. For the same reason, it is also irrelevant whether finite or infinite ratcheting is present, which is why a strict distinction between the two is omitted in the following.

This finding has implications for the choice of a material model for the calculation of elastic-plastic strains. So for this purpose models may also be used, which in principle cannot predict infinite ratcheting and tend to underestimate finite ratcheting, e.g., pure kinematic hardening without recovery terms. This deficiency should, however, be compensated either by reducing the maximum allowable strains or by appropriately modifying material parameters obtained by curve fitting, e.g., artificially reducing the tangent modulus  $E_t$ .

## 2.9 Analysis Methods

To obtain the elastic-plastic strains that are necessary for fatigue and ratcheting proof work, different methods are possible. Some provide only information on the range of strains for the fatigue check, and are not applicable to determining the accumulated strains for the ratcheting proof.

### 2.9.1 Fictitious Elastic Analysis and Correction Factors

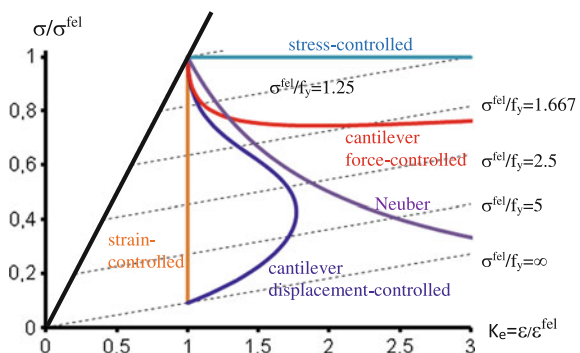
This method calculates the stress range for each pair of loads through adoption of linear elastic material behavior, and the resulting equivalent fictitious elastic strain range is multiplied with a plastic strain enhancement factor that can be taken from design codes. In many cases the plastic strain enhancement factor  $K_e$  (“ $K_e$ -factor””) of the ASME Code is being used, e.g., in [9]. A critical assessment of this factor can be found in [16]. Other proposals go back to Neuber [18], who has dealt with elastic-plastic strain concentration at sharp notches. A number of other proposals were developed by, amongst others, Hübel [16], Roche [19], and Seshadri [20], which partly entered into French and German design codes.

Generally, however, it is difficult to reflect adequately the complex elastic-plastic behavior depending on the material behavior, component geometry, load configuration, level of loading, etc., by a factor. This concept is historical and dates back to periods when the finite element method was not even available for linear calculations in engineering practice. From today’s perspective, this factorial approach is for general use, apart from special configurations of component geometry and kinds of loading, to be considered not very well founded on continuum mechanics. It draws its justification mainly from the fact that a rich experience in the application of this concept is available in narrowly circumscribed design situations.

Figure 2.35 shows some solutions for the plastic strain enhancement factor  $K_e$  for linear hardening ( $C/E = 0.1$ ). Shown in dashed lines are the material curves for different yield stresses or, because of the normalization, ultimately for different load levels, expressed using the fictitious elastic calculated stress  $\sigma^{\text{fel}}$ . The five colored lines show the dependence of the plastic strain enhancement factor  $K_e$  on the stress level because of stress redistribution: The curves for the limit behavior of a stress-controlled load (the stress is independent of the behavior of the material) and for the limit behavior of a strain-controlled load (the strain is independent of the behavior of the material) are horizontal or vertical.

Furthermore, the Neuber hyperbola is shown. It results from the requirement that the product of stress and strain is independent of the material behavior:

**Fig. 2.35** Examples of plastic strain enhancement with linear kinematic hardening material ( $C/E = 0.1$ ) under monotonic loading





$$\sigma \cdot \varepsilon(\sigma, f_y, C/E) = \text{const.} \neq f(C/E) \quad (2.29)$$

which therefore also applies to  $C/E \rightarrow \infty$  and thus to elastic behavior:

$$\sigma \cdot \varepsilon(\sigma, f_y, C/E) = \sigma^{\text{fel}} \cdot \varepsilon^{\text{fel}}. \quad (2.30)$$

In addition the solution for a cantilever beam under force- or displacement-controlled concentrated load at its free end, already mentioned in Sect. 1.1, is obtained from [16] and accordingly processed in Fig. 2.35.

The fictitious elastic stresses can be obtained with relatively little effort. This is true even for transient thermal loading in which the stresses must be determined for many points in time in order to identify those two points in time associated with the maximum range of stress or strain by subsequent post-processing. However, the determination of the relevant plastic strain enhancement factor in the context of the post-processing of finite element analyses can be quite costly, such as when the factor is based on the linearization of nonlinear elastic stress distributions across the wall thickness [9]. This is because the linearizations must be made to very many points in time at many cross-sections of a structure for transient loading. Finally, the location of the maximum fictitious elastically calculated stress range is not necessarily identical to the location of the maximum plastic strain enhancement factor, nor to the location of the maximum product of stress range and plastic strain enhancement factor.

Possible effects of mean strains or mean stresses on the fatigue usage cannot be captured with such factors that are purely related to strain ranges.

For the estimation of cyclically accumulated strain, such correction factors applied to elastically calculated stresses are unknown, so that an extension of this factorial concept to ratcheting is not possible.

## 2.9.2 Incremental Elastic-Plastic Analysis

In the incremental elastic-plastic analysis a predetermined load histogram is calculated step by step. To do this, an elastic-plastic material model is required, which is suitable for the description of loading and unloading at multiaxial stress states with varying ratios of the stress components, and which is based on the characteristics treated in Sect. 1.2, e.g., the Besseling or the Chaboche model, etc. Apart from academic examples or uniaxial tension-compression tests for the identification of material parameters, this is possible only by means of implementing these models in finite element programs.

As can hereby be identified which portions of the volume (zones) of a structure are plastically and which are not, it is also called the theory of plastic zones – in contrast to the theory of plastic hinges or the yield line theory, which allow plastic deformation to occur only in discrete cross-sections, thus disregarding local plastic straining in sections that are only partly plastic, e.g., in notches. Furthermore, in application of the theory of plastic hinges and the yield line theory, usually only

linear elastic-perfectly plastic or rigid plastic behavior is assumed. Hardening is thus disregarded, which makes sense for the calculation of load conditions produced by monotonic loading for some materials, but not for cyclically varying loads (cf. Sect. 1.2.5).

The term “incremental” refers not only to the fact that a load histogram needs to be divided into a sequence of monotonic loading changes, i.e., into a number of half cycles, but also that the flow law at Eq. (1.18) is formulated differentially. This can therefore, as already mentioned in Sect. 1.2.4, in general not be integrated in closed form, so that the change in load must be further divided into small sections (increments) within a half cycle and, because of the resulting path dependence of the loading process, for each of these intermediate states, a solution must be obtained. This can only be done iteratively because of the nonlinearity of the problem, because the finite element method is ultimately based on the creation and solution of linear systems of equations, and the linear system, which simulates the nonlinear problem adequately, without violating equilibrium conditions, must be found iteratively, usually with the help of Newton–Raphson iterations. With each change in load it is first assumed that this is connected with linearly elastic behavior. The stresses lying outside the yield surface (trial stress) are then projected to the yield surface (radial return method).

To capture this full path dependence of plastic structural behavior, a high computational effort is required. Each of  $l$  half cycles is to be subdivided into a number of  $s$  substeps, each calling for  $i$  equilibrium iterations. How many half cycles must be calculated until shakedown is achieved, how many substeps are required in each half cycle, and how many equilibrium iterations in each substep depend on the specific circumstances (component geometry, finite element mesh, load type, load level, material model, desired convergence tolerances, etc.) and varies greatly. To get, for example, the histograms of Fig. 2.34, a system of equations was set up and used to solve about  $l \times s \times i = 36 \times 10 \times 2 = 720$  times, which corresponds to the numerical effort of performing 720 linear elastic analyses.

If the sequence of different loadings is not known by in-service monitoring, a conservative load histogram must be developed first, which can also be associated with high computational effort.

An incremental analysis is the only method by which it can be determined how many cycles are required to achieve approximately the shakedown state, or how many cycles are required to reach a certain strain level.

### 2.9.3 Twice-Yield Method

The estimation of elastic-plastic strain by means of factorial correction of fictitiously elastic calculated stress (Sect. 2.9.1) and performing incremental cyclic analyses with an elastic-plastic material model (Sect. 2.9.2) represent the extreme approaches to determine elastic-plastic strains. Although one requires only little computational effort but is usually associated with unsatisfactory quality of the results, with the other, depending on the choice of an appropriate material model,

theoretically the best quality of results is achievable, but only with very high computational effort.

There is therefore a need for appropriate simplifications which lead to a compromise between quality of the results and computational effort required. It may be necessary to distinguish between methods that provide only an estimate of the strain range for use in a fatigue analysis and those which, in addition, also permit approximations for the accumulated strains (direct methods, Sect. 2.9.4).

One way to determine the strain range alone is the so-called twice-yield method of Kalnins [21]. After that, the strain range between the extremes of the two load conditions in the state of shakedown can approximately be determined by a monotonic incremental analysis by applying the load range as a monotonous load and calculating the structural response incrementally with an elastic-plastic material model. The material parameters have to be adapted to the cyclic stabilized stress-strain hysteresis. For a material without cyclic hardening and bilinear stress-strain curve, for example, the yield stress is doubled (hence the name), but the elastic modulus and the tangent modulus  $E_t$  is maintained.

This approach can lead to a good approximation for the strain range if the local and directional stress redistribution is not particularly pronounced, the temperature dependence of the material parameters plays no major role, and mean stress or mean strain effects need not be determined [22].

The twice-yield method is not applicable for the determination of the accumulated strain required for a ratcheting proof.

### 2.9.4 Direct Methods

So-called “direct methods” are intended to identify the state of shakedown without having to calculate a load histogram cycle by cycle incrementally. There is therefore no load histogram needed but only a load domain, which is multidimensional in general, containing all possible states and sequences of loads.

Direct methods are dealing with different questions:

- Which increase of the load, so what load factor, is possible in a specified load domain, just to guarantee shakedown?
- What stresses (strain, deformation, etc.) and which ranges is a structure experiencing in the shakedown state?

Different analysis methods are required to answer these questions. Some of these methods only allow the determination for which load intensity shakedown can be achieved, and what the nature of this shakedown state is (elastic or plastic shakedown), without having to determine the accumulated strains or strain ranges associated. If only two load states are involved in the cyclic loading, the result to be obtained corresponds to that of a ratcheting-interaction diagram. Their advantage is, however, to allow such statements for multiple load conditions, i.e., in a multi-dimensional load domain.

For this purpose use is made of so-called shakedown theorems:

- Either of the static shakedown theorem of Melan, known as the “lower bound theorem”, providing a lower and thus conservative bound of the load factor.
- Or of the kinematic shakedown theorem of Koiter, known as the “upper bound theorem”, providing an upper and thus non-conservative bound of the load factor.

The bounding character stems from the fact that, by analogy with the static and kinematic bounding theorems for plastic limit loads, solutions are sought that do not necessarily satisfy the field equations and the material law simultaneously. There are numerous references to both variants. Basics and numerous references are found in [4, 15, 23, 24], for example. Ultimately, the optimum fields of residual stresses or kinematic variables are sought, for which the structural behavior is formulated as a mathematical optimization problem [25, 26]. Mostly, linear elastic-perfectly plastic material behavior is assumed, but there are also extensions to capture unlimited linear, limited linear, or nonlinear kinematic hardening. Further extensions are related to temperature-dependent material data, dynamic loads, and the formulation of equilibrium conditions for the deformed system. The required computational effort for solving the optimization problem (mathematical programming) can be very high, depending on the finite element model because of the number of restrictions.

There are also proposals for direct methods in which, unlike the optimization problems mentioned above, the boundary value problem of structural mechanics is completely dissolved, i.e., all field equations (equilibrium and compatibility) and the yield condition are simultaneously fulfilled. Such methods have the advantage that they also provide information about deformations, displacements, etc., present in the state of shakedown, i.e., for all quantities that could otherwise be obtained by an incremental analysis of a load histogram. Because these quantities are required for a life assessment analysis in the sense of Sect. 2.8, such methods are, in principle, applicable both for a fatigue proof as well as for a ratcheting proof. Those methods are “direct” insofar as they directly aim at the shakedown state without performing a step-by-step analysis of a load histogram and therefore potentially require less numerical effort.

As the first limitation, it is already apparent that the path dependence of plastic behavior is lost. Likewise, it cannot be determined how many loading cycles are required until the shakedown state is reached. Also, the shape of the stress-strain hysteresis in the state of plastic shakedown cannot readily be obtained, which, however, is not necessarily a significant loss of information in strain-based fatigue analyses, because the dissipated energy does not enter there. As compensation for fully resolving the boundary value problem, other simplifications are introduced, which ultimately lead to a blurring of the results. A widely used simplification is to disregard the material hardening. So the results are estimates that differ from those obtained by an incremental analysis with a more realistic material model. This is the price that must be paid for this kind of simplified analysis method.

Amongst them are those methods based on an iterative sequence of linear elastic analyses with spatially varying Young's modulus, sometimes called EMAP (elastic modulus adjustment procedures). These include the Generalized Local Stress–Strain (GLOSS) Method of Seshadri [20, 27], the Elastic Compensation Method (ECM) of Mackenzie [28], and the Linear Matching Method (LMM) of Ponter and Chen [29, 30] (which still wasn't termed LMM in the first-mentioned publication). The GLOSS method can approximate the strain range in the state of shakedown, taking into account the material hardening, but cannot be used to predict accumulated strains. The ECM supplies the load factors in the shakedown state for non-hardening material, but neither strain ranges nor accumulated strains. The LMM applies only to non-hardening materials and supplies the strain ranges in the state of shakedown and the increment of strain per cycle when ratcheting occurs, which is a constant value because of the lack of hardening.

As direct methods, not belonging to the EMAP family, the Large Time Increment Method (LATIN) of Ladevèze [31, 32] and the Residual Stress Decomposition Method (RSDM) of Spiliopoulos and Panagiotou [33, 34] should be mentioned here.

A more detailed discussion of the methods listed, for example in relation to the achievable accuracy of the results, the required computational effort, the ability to model temperature dependent material behavior, taking into account multi-dimensional load domains, etc., is beyond the scope of this book by far.

Instead, another direct method, known as Zarka's method in the literature, and which serves as basis for the Simplified Theory of Plastic Zones, is presented in the following chapters in detail. As is seen there, a solution is sought iteratively through a series of successive elastic analyses. The theoretical basis and the procedure for doing this, however, differ greatly from the methods mentioned above. The aim is to estimate strain ranges and accumulated strains in the shakedown state, taking into account the hardening of the material.

---

## References

1. Miller, D.R.: Thermal-stress ratchet mechanism in pressure vessels. *ASME J. Basic Eng.* **81**, 190–196 (1959)
2. Mulcahy, T.M.: An assessment of kinematic hardening thermal ratcheting. *Trans. ASME J. Eng. Mater. Technol.* **96**(3), 214–221 (1974)
3. Jiang, W., Leckie, F.A.: A direct method for the shakedown analysis of structures under sustained and cyclic loads. *J. Appl. Mech.* **59**, 251–260 (1992)
4. Ponter, A.R.S.: Shakedown and Ratchetting Below the Creep Range, CEC Report EUR8702 EN. European Commission, Brussels (1983)
5. ANSYS Release 14.5, ANSYS Inc. Canonsburg, USA (2012)
6. Owen, R.J., Prakash, A., Zienkiewicz, O.C.: *Finite Element Analysis of Non-Linear Composite Materials by Use of Overlay Systems, Computers and Structures*, vol. 4, pp. 1251–1267. Pergamon Press, New York (1974)
7. Wolters, J., Majumdar, S.: *A three-bar Model for Ratcheting of Fusion Reactor First Wall*. Argonne National Laboratory, Argonne, Illinois (1994)

8. Hübel, H.: Basic conditions for material and structural ratcheting. *Nucl. Eng. Des.* **162**, 55–65 (1996)
9. Sicherheitstechnische Regel des KTA, KTA 3201.2. Komponenten des Primärkreises von Leichtwasserreaktoren, Teil 2: Auslegung, Konstruktion und Berechnung. Fassung 6/96 (including correction from BAnz. Nr. 129, 13.07.2000). Office of the KTA c/o Bundesamt für Strahlenschutz, Salzgitter (2000)
10. Bree, J.: Elastic-plastic behaviour of thin tubes subjected to internal pressure and intermittent high-heat fluxes with application to fast-nuclear-reactor fuel elements. *J. Strain Analysis* **2**(3), 226–238 (1967)
11. Hill, R.: *The Mathematical Theory of Plasticity*, pp 292–294. Oxford University Press, London (1950)
12. Sartory, W.K.: Structural Design for Elevated Temperature Environments – Creep, Ratchet, Fatigue, and Fracture Effect of peak thermal strain on simplified ratchetting analysis procedures, *ASME Proceedings, PVP* **163**, 31–38 (1989)
13. Burth, K., Brocks, W.: *Plastizität: Grundlagen und Anwendungen für Ingenieure*. Vieweg, Braunschweig/Wiesbaden (1992)
14. Hübel, H.: Bemerkungen zur Ausnutzung plastischer Querschnitts- und Systemreserven. *STAHLBAU* **72**(12), 844–852 (2003)
15. Sawczuk, A.: shakedown analysis of elastic-plastic structures. *Nucl. Eng. Des.* **28**, 121–136 (1974)
16. Hübel, H.: Plastische Dehnungserhöhungsfaktoren in Regelwerken und Vorschlag zur Etablierung angemessenerer Faktoren. Gesamthochschule Kassel, Institut für Mechanik, Mitteilung Nr. 4 (Dissertation) (1985)
17. Haibach, E.: *Betriebsfestigkeit. Verfahren und Daten zur Bauteilberechnung*. Springer, Berlin/Heidelberg (2006)
18. Neuber, H.: Theory of stress concentration for shear strained prismatical bodies with arbitrary, nonlinear stress-strain law. *Trans. ASME, J. Appl. Mech.* **28**(4), 544–550 (1961)
19. Roche, R.L.: Practical procedure for stress classification. *Int. J. Pres. Ves. Piping* **37**, 27–44 (1989)
20. Seshadri, R.: The Generalized Local Stress Strain (GLOSS) Analysis – Theory and Applications. *Trans. ASME J. Pressure Vessel Technol.* **113**, 219–227 (1991)
21. Kalnins, A.: Fatigue analysis of pressure vessels with twice-yield plastic FEA. *ASME PVP* **419**, 43–52 (2001)
22. Hübel, H., et al.: Performance study of the simplified theory of plastic zones and the Twice-Yield method for the fatigue check. *Int. J. Press. Vessels Pip.* **116**, 10–19 (2014). doi:[10.1016/j.ijpvp.2014.01.003](https://doi.org/10.1016/j.ijpvp.2014.01.003)
23. Ponter, A.R.S., Karadeniz, S., Carter, K.F.: The computation of shakedown limits for structural components subjected to variable thermal loading – Brussels diagrams, CEC Report EUR 12686 EN. European Commission, Brussels (1990)
24. König, J.A., Maier, G.: Shakedown Analysis of Elastoplastic Structures: A Review of Recent Developments. *Nucl. Eng. Des.* **66**, 81–95 (1981)
25. Heitzer, M., Staat, M.: FEM-computation of load carrying capacity of highly loaded passive components by direct methods. *Nucl. Eng. Des.* **193**, 349–358 (1999)
26. Staat, M., Heitzer, M.: LISA – a European project for FEM-based limit and shakedown analysis. *Nucl. Eng. Des.* **206**, 151–166 (2001). doi:[10.1016/S0029-5493\(00\)00415-5](https://doi.org/10.1016/S0029-5493(00)00415-5)
27. Seshadri, R.: residual stress estimation and shakedown evaluation using GLOSS analysis. *J. Press. Vessel Technol.* **116**(3), 290–294 (1994). doi:[10.1115/1.2929590](https://doi.org/10.1115/1.2929590)
28. Mackenzie, D., Boyle, J.T., Hamilton, R.: The elastic compensation method for limit and shakedown analysis: a review. *Trans. IMechE J. Strain Anal. Eng. Des.* **35**(3), 171–188 (2000)
29. Ponter, A.R.S., Carter, K.F.: Shakedown state simulation techniques based on linear elastic solutions. *Comput. Methods Appl. Mech. Eng.* **140**, 259–279 (1997)
30. Chen, H.: Linear matching method for design limits in plasticity, computers. *Materials Continua. Tech. Sci. Press* **20**(2), 159–183 (2010)

31. Ladevèze, P.: *Nonlinear Computational Structural Mechanics – New Approaches and Non-Incremental Methods of Calculation*. Springer, New York (1999)
32. Maier, G., Comi, C., Corigliani, A., Perego, U., Hübel, H.: Bounds and estimates on inelastic deformations, Commission of the European Communities, contract RA1-0162-I and RA1-0168-D, Report EUR 16555 EN. European Commission, Brussels (1992)
33. Spiliopoulos, K.V., Panagiotou, K.D.: A direct method to predict cyclic steady states of elastoplastic structures. *Comput. Methods Appl. Mech. Eng.* **223–224**, 186–198 (2012)
34. Spiliopoulos, K.V., Panagiotou, K.D.: The residual stress decomposition method (RSDM): a novel direct method to predict cyclic elastoplastic states. In: Spiliopoulos, K., Weichert, D. (Eds.) *Direct Methods for Limit States in Structures and Materials*, pp 139–155. Springer Science + Business Media, Dordrecht (2014). doi:[10.1007/978-94-007-6827-7](https://doi.org/10.1007/978-94-007-6827-7)

<http://www.springer.com/978-3-319-29873-3>

Simplified Theory of Plastic Zones

Based on Zarka's Method

Hübel, H.

2017, XV, 318 p. 231 illus., 178 illus. in color.,

Hardcover

ISBN: 978-3-319-29873-3